

Influence of long-range transported Asian dust on cirrus cloud formation over central Pacific

Yun He^{1,2*}, Huijia Shen², and Zhenping Yin³

¹Leibniz Institute for Tropospheric Research, 04318 Leipzig, Germany

²School of Electronic Information, 430072 Wuhan, China

³School of Remote Sensing and Information Engineering, 430072 Wuhan, China

Abstract. Cirrus clouds play a vital role in regulating the global radiative balance and climate, with their net radiative forcing determined by microphysical properties, which are strongly related to the ice-nucleating mechanisms, i.e., heterogeneous or homogeneous nucleation. However, there are lack of direct observational cases regarding the influence of long-range transport of Asian dust on primary ice formation in cirrus over the Pacific. Here we report on two such dust-cirrus interaction cases over the central Pacific with the combined observations of space-borne Cloud-Aerosol Lidar with Orthogonal Polarization (CALIOP) and Cloud Profiling Radar (CPR). Both cases show good agreement (within an order of magnitude) of in-cloud ICNC and nearby dust-related INP concentration (INPC) values, indicating that dust-induced heterogeneous nucleation is dominated in ice formation. This study shows that the natural supply of effective INPs to the upper troposphere can modulate the microphysical properties of cirrus clouds by acting as INPs and further influence on global climate. This information is useful for parameterizing ice formation in climate models.

1 Introduction

Cirrus clouds are ice clouds that widely exist in the upper troposphere and lower stratosphere when temperatures are lower than $-38\text{ }^{\circ}\text{C}$, and play a vital role in global climate by regulating the radiative balance of the Earth [1]. Ice crystals in cirrus clouds form via either homogeneous or heterogeneous, causing a large uncertainty in general circulation models [2]. Homogeneous nucleation usually produces small ice crystals with a larger ice crystal number concentration (ICNC) and tends to result in a net warming effect; in contrast, heterogeneous nucleation forms crystals with larger size but lower ICNC, which may weaken the warming effect [3]. It is still difficult to conclude the exact influence of cirrus clouds on global climate currently [4].

Dust aerosols are one of the most efficient ice-nucleating particles (INPs) in the middle and upper troposphere. Dust-triggered ice production is of great importance in global cirrus cloud formation [5]. The dust-cirrus interactions are widely studied for terrestrial and offshore regions [6]. However, over extensive ocean regions, few cirrus cloud observations are reported and the formation of cirrus clouds has not yet been investigated [7]. The maritime atmospheric environment is usually clean with an aerosol optical depth of <0.1 [8]; nevertheless, the average frequency of occurrence of cirrus clouds observed by CloudSat/CALIPSO can be as high as 0.3-0.4 [9]. Is cirrus formation only attributed to

homogeneous freezing over the ocean? In general, Asian dust plumes can undergo long-range transport to the North Pacific, Northern America, and even full circle around the globe [10]. Hence, the possible influence of transoceanic dust particles on cirrus cloud formation should be considered. Further, it is also of great interest to quantitatively examine whether transoceanic dust plumes can provide high-level INPC values farther over the central Pacific and thus alter the dominant ice nucleating mechanism over the remote ocean. This will help our understanding the potential dust-cirrus interactions over the remote ocean.

This study examines the potential influence of long-range transported Asian dust on cirrus cloud formation over remote oceanic regions based on the observations of CALIOP and CPR. Two cases near Midway Island (28.21°N , 177.38°W), located in the central Pacific within the transpacific dust belt, are studied in detail [11].

2 Data and Methodology

2.1 CALIOP observational data

The spaceborne polarization lidar CALIOP on the CALIPSO satellite was utilized to obtain the vertical profiles of optical properties of cirrus clouds and dust layers. Level-1 product was used to provide the 532-nm total attenuated backscatter coefficient and volume depolarization ratio to examine the spatial distribution

* Corresponding author: hey@tropos.de; heyun@whu.edu.cn

of dust and cirrus layers. Level-2 aerosol profile product was used to obtain the vertical profiles of the aerosol extinction coefficient, particle depolarization ratio (PDR), and atmospheric volume description to study the optical and microphysical properties of dust and cirrus layers in detail [12]. We can obtain the vertical feature mask (VFM), aerosol subtype, and cloud subtype to identify ‘cirrus’ and ‘dust’ (including dust and polluted dust) from the ‘atmospheric volume description’. In addition, the meteorological data including the temperature, pressure, and relative humidity profiles along the satellite tracks were derived from the MERRA-2 reanalysis data.

2.2 ICNC derived from the DARDAR dataset

DARDAR dataset combines the co-located and quasi-simultaneous detection of the CALIOP onboard CALIPSO and the CPR onboard CloudSat [13]. DARDAR-Nice profile product was employed to provide the profiles of in-cloud ICNC (n_{ice}) for ice crystals having diameters larger than 5 μm , 25 μm , and 100 μm , respectively [14,15]. Both products possess a 60-m vertical resolution and a 1.7-km horizontal resolution.

2.3 Dust-related INPC obtained with POLIPHON method

The POLIPHON method was adopted to compute the dust-related INPC and dust mass concentration values [16,17]. It extracted the dust extinction coefficient α_d from the aerosol extinction coefficient α_p provided by CALIOP level-2 data using the one-step approach, in which particles are divided into dust and non-dust components by the particle depolarization ratio [16]. The employed meteorological parameters are integrated within the CALIOP level-2 aerosol profile product. Here lidar ratio for dust LR_d was assumed to be 45 sr [18]. Then, the dust extinction coefficient can be converted into cloud-relevant parameters, including the dust mass concentration M_d , particle number concentration with a radius >250 nm $n_{250,d}$, and particle surface area concentration S_d and $S_{100,d}$ (with a radius >100 nm), by multiplying the conversion factors $c_{v,d}$, $c_{250,d}$, $c_{s,d}$ and $c_{s,100,d}$. He et al. [19] calculated the conversion factors over Midway Island. For dust-related INPC computation, we applied the parameterization scheme U17-D (Eq. (7) of Ullrich et al. 2017) [20] for deposition freezing.

2.4 HYSPLIT model

To examine the potential regions of dust origin, the HYSPLIT (Hybrid Single-Particle Lagrangian Integrated Trajectory) [21] was used to compute the backward trajectories of the air masses originating at Midway Island.

3 Results

3.1 Case on 5 May 2010

Figure 1 shows the CALIOP 532-nm total attenuated backscatter coefficient (TAB) and volume depolarization ratio δ_v , and vertical feature mask, cloud subtype, and aerosol subtype on 5 May 2010. A cirrus cloud appeared at 8.3-10.0 km with δ_v exceeding 0.3 and strong TAB. It was embedded in a dust layer with δ_v values of 0.1-0.2 and weaker TAB; thus, ice formation in the cirrus cloud was possibly influenced by dust particles via heterogeneous nucleation. The dust plume originated from the Asian dust source regions two days earlier as simulated by the HYSPLIT model (see Fig. 2).

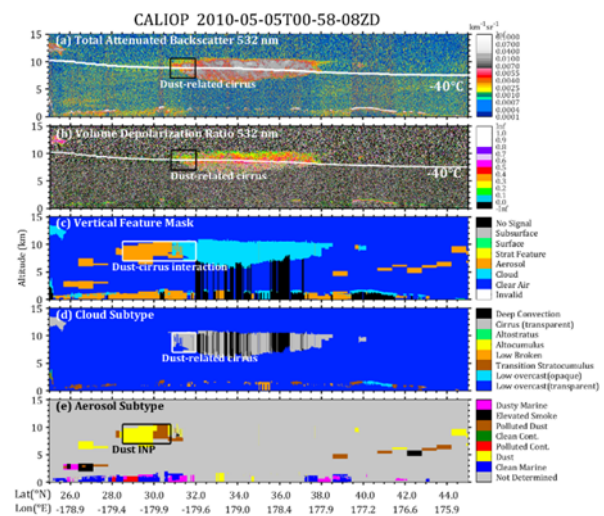


Fig. 1. CALIPSO altitude-orbit cross section of the level-1B 532-nm (a) total attenuated backscatter coefficient, (b) volume depolarization ratio product, and level-2 (c) vertical feature mask, (d) cloud subtype, and (e) aerosol subtype product on 5 May 2010.

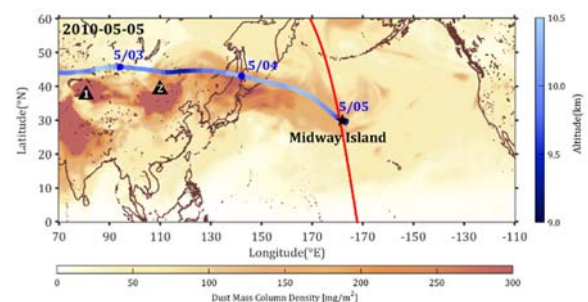


Fig. 2. The dust mass column density on 5 May 2010 from MERRA-2 data together with the 3-day backward trajectories simulated by the HYSPLIT model. The red line denotes the footprint of the CALIPSO satellite.

As seen in Fig. 3, the dust layer at 9.0-9.8 km has a mean dust extinction coefficient of 25.6 Mm^{-1} , suggesting that a large number of dust particles can still be well-retained within the plume during their long-range transoceanic transport. PDRs generally range from 0.2 to 0.3, indicating the inclusion of pure dust particles. Figure 3e presents the dust-related INPC profiles calculated with U17-D parameterization. At

altitudes of 9.0-9.8 km, the layer-average dust-related INPCs are 7.2 L^{-1} for an assumed ice saturation ratio S_i of 1.15, 96.3 L^{-1} for S_i of 1.25, and 642.6 L^{-1} for S_i of 1.35. As a comparison, in-situ measurements over Florida observed a slightly higher peak INPC of 300 L^{-1} (at a temperature of $-36 \text{ }^\circ\text{C}$ and RH_i of 123%) in the dust layer transported from the Saharan desert [22,23]. INPC values reach a maximum at the cloud top and then gradually decrease as the altitude decreases since INPCs strongly depend on the temperature.

Figure 3e also provides the ICNCs larger than $5 \mu\text{m}$, $25 \mu\text{m}$, and $100 \mu\text{m}$ from the DARDAR-Nice product, as denoted by $n_{\text{ice},5 \mu\text{m}}$, $n_{\text{ice},25 \mu\text{m}}$ and $n_{\text{ice},100 \mu\text{m}}$, respectively. All these ICNC values show an enhancement around 9.5-km altitude, which is approximately 0.5 km below the cloud top. For cirrus clouds within the latitude of $31.5\text{-}31.8^\circ\text{N}$ at 9.0-9.8 km, the average ICNCs are 140.7 L^{-1} for $n_{\text{ice},5 \mu\text{m}}$, 60.4 L^{-1} for $n_{\text{ice},25 \mu\text{m}}$, and 7.1 L^{-1} for $n_{\text{ice},100 \mu\text{m}}$. Ansmann et al. [24] observed ICNC values of 4.3-39 L^{-1} in cirrus clouds. Cziczo et al. [25] reported that the ICNC values for heterogeneous freezing are typically 1-100 L^{-1} . Thus, the ICNC values observed in this case reflect the typical situation of heterogeneous nucleation within the cirrus clouds. Above 9 km, the coldest part of the cirrus clouds with temperatures $< -40 \text{ }^\circ\text{C}$, homogeneous nucleation is generally considered to take place because it is usually very clean there. However, abundant dust INPs were provided here by the long-range transpacific dust plume. Therefore, when dust particles come across this region with a high moisture level, it is conducive to the occurrence of heterogeneous nucleation and subsequent suppression of homogeneous nucleation by consuming available water vapor [26]. Comparing the in-cloud ICNC and dust-related INPC values, U17-D-derived INPCs with S_i of 1.15 well agree with in-cloud $n_{\text{ice},5 \mu\text{m}}$ (ICNC-to-INPC ratio of 0.9). Additionally, INPCs with S_i of 1.25 are closer to $n_{\text{ice},25 \mu\text{m}}$ (ICNC-to-INPC ratio of 0.7), therefore, heterogeneous freezing should solely be responsible for ice formation in the cirrus cloud.

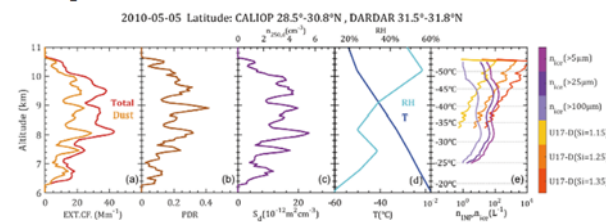


Fig. 3. Profiles of the 532-nm (a) dust and total extinction coefficient, (b) particle depolarization ratio, (c) large particle number concentration and surface area concentration, (d) relative humidity RH and temperature T, and (e) n_{INP} and n_{ice} on 5 May 2010.

3.2 Case on 27 April 2008

The second case was observed on 27 April 2008 as shown in Fig. 4. Ice clouds appeared between $27.1\text{-}28.3^\circ\text{N}$ at 10.0-11.4 km with relatively intense TAB and a large δ_v of > 0.3 and were embedded in a dust plume with δ_v values of 0.1-0.2 and a relatively

weaker TAB. ‘Cirrus clouds’ can be seen with ‘dust’ and ‘polluted dust’ in the vicinity. The 5-d backward trajectories were computed by the HYSPLIT model to confirm that the dust plume originated from the Asian dust source regions three days earlier (see Fig. 5).

As seen from Fig. 6, CALIOP aerosol extinction coefficient and PDR profiles for the dust layers at latitudes of $27.1\text{-}28.3^\circ\text{N}$ were utilized to estimate the effective concentration of dust INPs near the cirrus clouds. For the dust layer at 10.2-11.4 km, δ_p takes a relatively small peak value of 0.15 at 10.5 km; while the dust extinction coefficient is on average 10.6 Mm^{-1} with a maximum of 33.7 Mm^{-1} . In addition, comparing the total and dust extinction coefficient, there is also a mass of non-dust aerosols carried within the dust plume, explaining the low δ_p values.

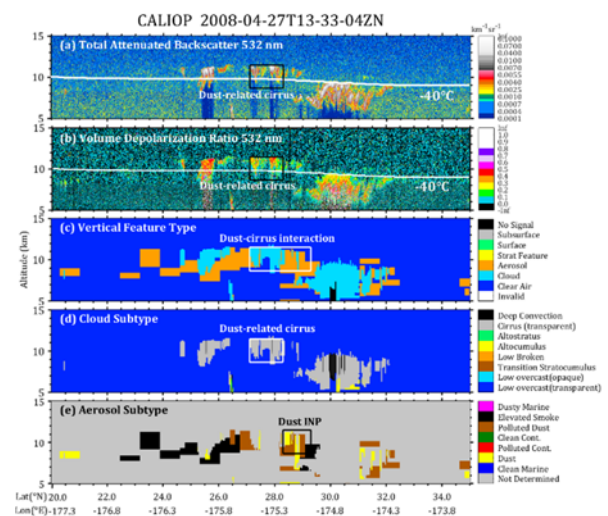


Fig. 4. Same as Fig. 1 but for 27 April 2008.

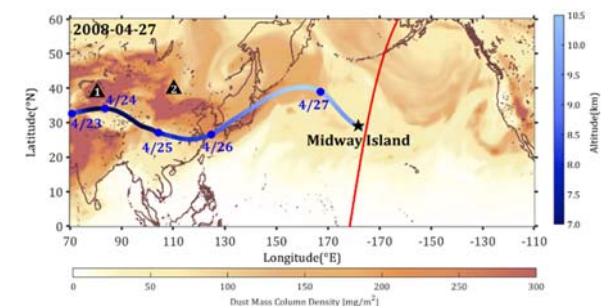


Fig. 5. Same as Fig. 2 but for 27 April 2008.

Cirrus clouds generally appeared at 10.2-11.4 km. The average dust-related INPCs with S_i of 1.15, 1.25, and 1.35 are 27.0 L^{-1} , 416.7 L^{-1} , and 3101.0 L^{-1} , respectively. For the cirrus clouds with latitudes of $27.8\text{-}28.2^\circ\text{N}$ at 10.2-11.4 km, the average ICNC values are 376.6 L^{-1} for $n_{\text{ice},5 \mu\text{m}}$, 167.7 L^{-1} for $n_{\text{ice},25 \mu\text{m}}$, and 20.0 L^{-1} for $n_{\text{ice},100 \mu\text{m}}$. An evident enhancement of ICNC values appeared at 10.2-11.4 km and reached the peak at $\sim 11.2 \text{ km}$. Comparing the dust-related INPCs with S_i of 1.25 with $n_{\text{ice},5 \mu\text{m}}$, they agree well with the in-cloud $n_{\text{ice},5 \mu\text{m}}$ with an ICNC-to-INPC ratio of 0.9. Besides, the U17-D-derived INPCs with S_i of 1.15 also agree well with the in-cloud $n_{\text{ice},100 \mu\text{m}}$ with an ICNC-

to-INPC ratio of 0.7. Therefore, it can be concluded that only heterogeneous nucleation may explain ice formation. These lower ICNC values together with good agreement between INCN and INPC confirm the transoceanic dust particles are non-negligible in cirrus formation via heterogeneous nucleation even over the central Pacific.

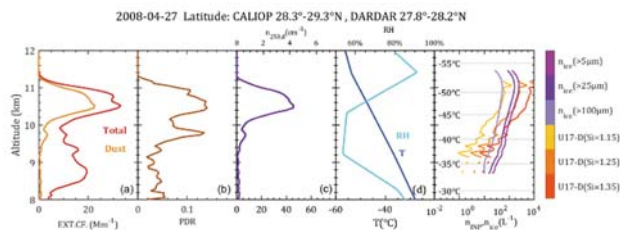


Fig. 6. Same as Fig. 3 but for 27 April 2008.

4 Conclusions

Two case studies are performed to prove that long-range transpacific Asian dust plumes can influence cirrus formation much farther over the central Pacific by providing a high level of INPC. The huge reservoir of INPs in the two cases originated from more intense Asian dust events caused by Mongolian anticyclones. Ice formation and microphysical properties of cirrus clouds over remote ocean regions can be regulated by the natural sources of INPs. At the upper troposphere, besides the long-range transported dust aerosols [27], sea spray particles originating from the sea surface, smoke aerosols from wildfire events, and volcanic-emitted aerosols also have a potential impact on the ice-nucleating regime as well as the radiative forcing of cirrus clouds over remote oceanic regions. The natural supply of INPs to the upper troposphere may modulate the microphysical properties of cirrus clouds by differentiating ice-nucleating regimes to induce a cooling effect on global climate. These aerosol-cirrus interactions over remote oceanic regions should be well considered in climate evaluation.

References

1. IPCC: Climate Change 2021, Cambridge University Press, Cambridge, United Kingdom and New York, NY, USA (2021)
2. M. Krämer, C. Rolf, A. Luebke, et al. *Atmos. Chem. Phys.*, **16**, 3463–3483 (2016)
3. P. DeMott, A. Prenni, X. Liu, et al. *Natl. Acad. Sci. USA*, **107**, 11217–11222 (2010)
4. V. Wolf, T. Kuhn, and M. Krämer. *Geophys. Res. Lett.*, **46**, 12565–12571 (2019)
5. K. Froyd, P. Yu, G. Schill, et al. *Nat. Geosci.*, **15**, 177–183 (2022)
6. T. Sakai, N. Orikasa, T. Nagai, et al. *J. Geophys. Res. Atmos.*, **119**, 3295–3308 (2014)
7. F. Cairo, M. De Muro, M. Snels, et al. *Atmos. Chem. Phys.*, **21**, 7947–7961 (2021)
8. A. Smirnov, B. Holben, D. Giles, et al. *Atmos. Meas. Tech.*, **4**, 583–597 (2011)
9. K. Sassen, Z. Wang, and D. Liu. *J. Geophys. Res.*, **113**, D00A12 (2008)
10. I. Uno, K. Eguchi, K. Yumimoto, et al. *Nat. Geosci.*, **2**, 557–560 (2009)
11. H. Shen, Z. Yin, Y. He, et al., *EGUsphere* [preprint] (2023)
12. A. Omar, D. Winker, C. Kittaka, et al. *J. Atmos. Ocean Tech.*, **26**, 1994–2014 (2009)
13. J. Delanoë, and R. J. Hogan. *Geophys. Res.*, **113**, D07204 (2008)
14. O. Sourdeval, E. Gryspeerdt, M. Krämer, et al. *Atmos. Chem. Phys.*, **18**, 14327–14350 (2018)
15. E. Gryspeerdt, O. Sourdeval, J. Quaas, et al. *Atmos. Chem. Phys.*, **18**, 14351–14370 (2018)
16. R.-E. Mamouri, and A. Ansmann. *Atmos. Meas. Tech.*, **7**, 3717–3735 (2014)
17. R.-E. Mamouri, and A. Ansmann. *Atmos. Chem. Phys.*, **15**, 3463–3477 (2015)
18. L. Peng, F. Yi, F. Liu, et al. *Opt. Express*, **29**, 21947–21964 (2021)
19. Y. He, Z. Yin, A. Ansmann, et al. *Atmos. Meas. Tech.*, **16**, 1951–1970 (2023)
20. R. Ullrich, C. Hoose, O. Möhler, et al. *J. Atmos. Sci.*, **74**, 699–717 (2017)
21. A. Stein, R. Draxler, G. Rolph, et al. *Bull. Amer. Meteor. Soc.*, **96**, 2059–2077 (2015)
22. P. DeMott, K. Sassen, M. Poellot, et al. *Geophys. Res. Lett.*, **30**(14), 1732 (2003)
23. P. DeMott, K. Sassen, M. Poellot, et al. *Geophys. Res. Lett.*, **36**, L07808 (2009)
24. A. Ansmann, R.-E. Mamouri, J. Bühl, et al. *Atmos. Chem. Phys.*, **19**, 15087–15115 (2019)
25. D. Cziczo, K. Froyd, C. Hoose, et al. *Science*, **340**, 1320–1324 (2013)
26. B. Kärcher, P. DeMott, E. Jensen, et al. *J. Geophys. Res. Atmos.*, **127**, e2021JD035805 (2022)
27. Y. He, Z. Yin, F. Liu, et al. *Atmos. Chem. Phys.*, **22**, 13067–13085 (2022)